Shock Waves (2007) 16:179–187
DOI 10.1007/s00193-006-0059-5

ORIGINAL ARTICLE

Interaction of a shock wave with a loose dusty bulk layer

B. C. Fan · Z. H. Chen · X. H. Jiang · H. Z. Li

Received: 7 September 2005 / Accepted: 11 July 2006 / Published online: 29 November 2006

Abstract The interaction of a planar shock wave with a loose dusty bulk layer has been investigated both experimentally and numerically. Experiments were conducted in a shock tube. The incident shock wave velocity and particle diameters were measured with the use of pressure transducers and a Malvern particle sizer, respectively. The flow fields, induced by shock waves, of both gas and granular phase were visualized by means of shadowgraphs and pulsed X-ray radiography with trace particles added. In addition, a two-phase model for granular flow presented by Gidaspow is introduced and is extended to describe such a complex phenomenon. Based on the kinetic theory, such a two-phase model has the advantage of being able to clarify many physical concepts, like particulate viscosity, granular conductivity and solid pressure, and deduce the correlative constitutive equations of the solid phase. The AUSM scheme was employed for the numerical calculation. The flow field behind the shock wave was displayed numerically and agrees well with our corresponding experimental results.

Keywords Shock wave · Dense two-phase flow · Granular temperature · ASUM scheme

PACS 47.40.-x

Communicated by L. Bauwens.

B. C. Fan (✉) · Z. H. Chen · X. H. Jiang · H. Z. Li
Laboratory of Transient Physics,
Nanjing University of Science and Technology,
Nanjing, 210094, China
e-mail: bcfan@mail.njust.edu.cn

1 Introduction

When a planar shock wave propagates over a thin dust layer, particles behind the shock wave are lifted up to form a dust cloud. Many experimental and numerical investigations have been performed on this phenomenon because of its practical significance to many kinds of industries. For example, Fletcher [1], Gelfand et al. [2], Fan and Li [3] performed similar experiments in a shock tube, and Li et al. [4], Thevand and Daniel [5], Katsunori et al. [6] attempted to simulate this phenomenon numerically.

If the height of dust layer is large enough, the wave patterns induced by the incident shock wave inside the powder have to be considered, then the above phenomenon will be more complex. Based on theoretical analyses, it can be deduced that when a shock wave passes over a loose particle mass the front of the leading shock wave front will be curved due to the different acoustic impedances between the gas and dusty mass, and like the thin dust layer case, a dust cloud behind the shock wave is formed. Furthermore, the transmitted shock wave is generated inside the dusty mass and the interface is deformd by the action of the shock waves. So far, few experiments have been published which deal with the phenomenon of a shock wave passing over a dusty mass. The traditional experimental optical techniques, even normal X-ray radiography cannot visualize the flow patterns inside the the dusty mass.

On other hand, some two-phase models appropriate for describing a dense gas–solid or a granular flow, in which particle–particle collisions dominate the flow rather than turbulent fluid–particle interactions, have been proposed. For example, based on the continuum

theory and the second law of thermodynamics, Baer and Nunziato [7] presented a two-phase reactive flow model (BN model) to describe a deflagration-to-detonation transition in a reactive granular material. With the introduction of Helmholtz free energy and by requiring the model to satisfy the entropy inequality (second law of thermodynamics), specific constitutive equations representing important aspects for granular materials were established. Later, Powers et al. [8] developed a more generalized model that incorporated most of the features of the BN model and included a set of specific constitutive relations. This model was introduced to model the combustion of granular particles. However, because of the lack of a two-phase theory with microstructural rigor, the constitutive relations defined in most current dense two-phase models, such as the pressure and sound speed of the solid phase, have no clear reason and physical meaning, and are determined usually by empirical data. With the definition of phase-frozen sound speed of a solid flow and neglecting configuration pressure, Zhang et al. [9] developed a heuristic model for the state equation of the solid flow. They incorporated it into the BN model to describe the rapid dispersal of inert solid particles caused by the detonation of a heterogeneous explosive.

In the present investigation, a special experimental measuring method has been developed by the combination of pulsed X-ray radiography and trace particles inside the dust bulk, which can display the flow field both of the gas and the dusty mass. Moreover, a dense two-phase flow model, based on the application of kinetic theory, developed by Gidaspow [10] is employed. In this model many physical concepts regarding the solid phase, such as particulate viscosity, granular conductivity and solid pressure are clarified. The "granular temperature" which relates to the oscillatory velocity of particles is defined to predict these random fluctuations of the solid phase. The constitutive equations of the solid phase are derived from the interactions of the fluctuating and the mean motions of the particles. These interactions give rise to an effective shear viscosity and predict the effective transport coefficients and the constitutive equations for the solid phase. The advection upstream splitting method (AUSM) [11], which has the advantage of efficiency in accurate capturing of shocks, contact discontinuities and requires no matrix operations, has been adopted for solving such dense two-phase flow equations. Calculated and measured results are in good agreement. The wave patterns inside both the gas and particle bulk mass induced by shock wave are discussed based on our experimental and calculated results

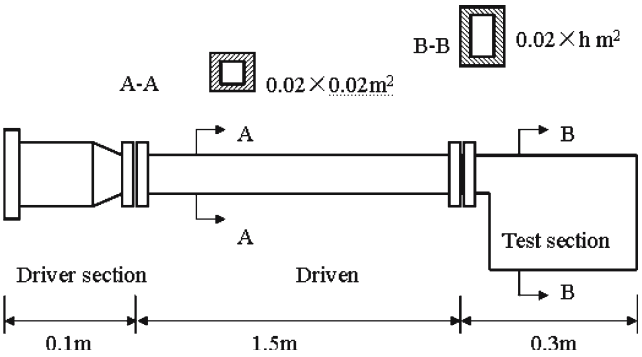

Fig. 1 Sechematic diagram of shock tube

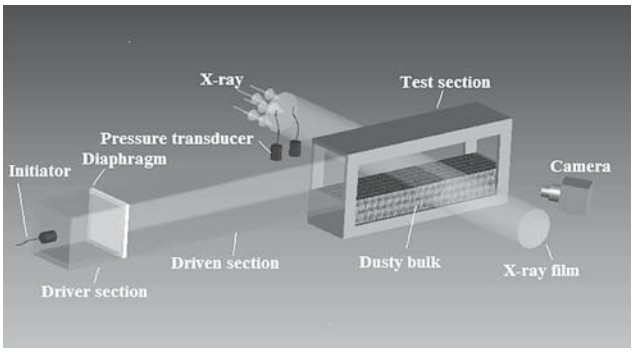

Fig. 2 Schematic of experimental set-up

2 Experimental investigation

2.1 Experimental set-up

Experiments were carried out in a horizontal shock tube which is shown in Fig. 1 and Fig. 2 shows the schematic of experimental set-up. The tube consists of a driver section, a driven section and a test section, which has the initial conditions of temperature $T = 300\,\mathrm{K}$ and pressure $P = 10^5\,\mathrm{Pa}$. The cross section of the shock tube is rectangular. The inside cross sectional area of the driver and driven section equals $0.02 \times 0.02\,\mathrm{m}^2$ (A-A in Fig. 1), and their length is 0.1 and 1.5 m, respectively. The test section, connected to the driven section of the shock tube, has a length of 0.3 m and cross sectional area of $0.02 \times h\,\mathrm{m}^2$ (B-B in Fig. 1). The height h is larger than 0.02 m, which can be modified based on the experimental requirement. The top inner wall of the driven tube is on the same level as that of the test chamber and the granular media in the test section is filled to the same level as the bottom of the driven section.

There is an initiator at the closed end of the driver section which is made of resistance wires. The surface of the wire is covered with solid propellant which is able to combust rapidly to produce high pressure inside the

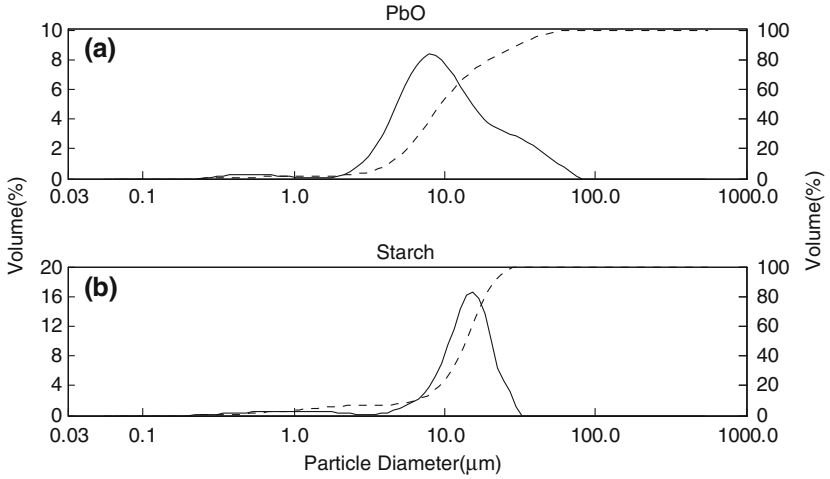

Fig. 3 Particle diameter distribution

driver section. A diaphragm was used to separate the driver and driven section. When the pressure inside the driver section is high enough, the diaphragm bursts and a shock wave forms and propagates along the driven section. Within the driven section, two pressure transducers were used for both measuring the pressure signal and average propagation velocity of the shock wave just before entering the test chamber. The first pressure transducer (P1) is located at a distance of 1.2 m from the diaphragm, and the second one (P2) is located 1.40 m from the diaphragm. In order to visualize the interaction process of the shock wave and granular media, two optical glass windows were installed on both sides of the test chamber. The powder which was deposited homogeneously inside the test chamber was made of ultra-fine starch particles.

For flow visualization, the normal high-speed optical shadowgraph technique was used to record the propagation front of a shock wave and dust entrainment of the shear layer behind the shock wave. The optical system consists of a spark light source, a Fresnel lens and a camera. The spark light source is triggered by the pressure transducer [3]. Usually, a normal light beam is barely able to penetrate through the dusty bulk mass, however, X-rays penetrate completely with little attenuation, so it is hard for either of them to display the distribution of particle density inside the dust. In present experiments, pulsed X-ray shadow photography was employed with the choice of PbO powder as the trace particles which absorb and attenuate the X-rays. After mixing homogeneously with the starch powder, the variation of trace particle density is considered the same as that of the powder density, therefore it can be used for indicating the variation of granular media density when the shock wave interacts with granular media.

2.2 Experimental results

The distributions of particle diameters and the material densities were measured by a Malvern Mastersizer, which is based on the laser diffraction method. The measured results are shown both in Fig. 3a and b for PbO and starch, respectively. The solid line corresponding to the left coordinate axis denotes the volume fraction of particles and the dashed line, corresponding to the right coordinate axis, shows the integration of the particle volume fraction. Our experimental measurement showed that the mean diameter d_p and material density ρ_s of the starch is about 15 μm and $1,100\,\mathrm{kg/m^3}$, respectively. For the PbO particles, the corresponding mean diameter and material density are $d_p = 9\mu\mathrm{m}$ and $\rho_s = 9,500\,\mathrm{kg/m^3}$, respectively. In our experiments, the initial bulk density of the particle mass $\alpha_s\rho_s$ was chosen as $520\,\mathrm{kg/m^3}$, where α is the volume fraction of the particle phase.

Typical measured pressure transducer signals are shown in Fig. 4. It is clear that the relative peak values measured by the two pressure transducers are almost equal. This means that the shock wave attenuation can be ignored and its propagation inside the tube may be considered to be steady during its propagation. The time for shock wave passage between the locations of two pressure transducers is about 202μs, and the average velocity of the incident shock wave for the present investigation can be calculated, which is of about 990 m/s. Our experimental results also showed that when the shock wave propagates over the dusty mass interface, the influence of the boundary layer of the wall behind the shock front may be ignored compared to that of the dusty mass interface.

Figure 5 displays both the shadowgraph of the shock wave propagating along the surface of the starch dust

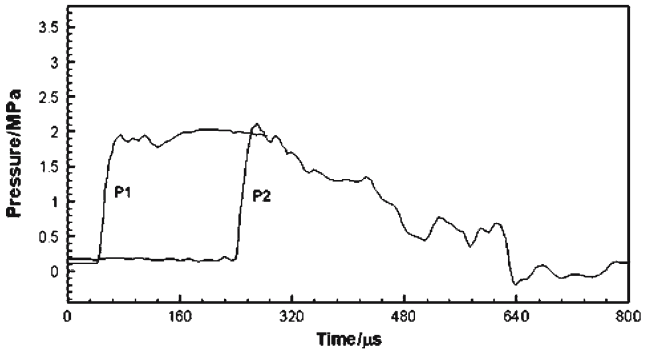

Fig. 4 Typical pressure records for shock velocity measurements

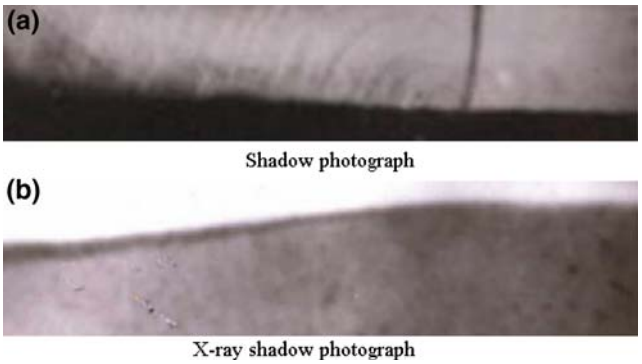

Fig. 5 Typical shadowgraph of interaction of shock wave and surface of starch dusty bulk

(Fig. 5a) and the X-ray photo of the flow field inside the dusty mass (Fig. 5b). This visualization clearly shows the interaction between the shock wave and dusty mass, the flowfield of the shear layer behind the shock wave and the wave structures both in air and granular media.

Figure 5a shows the shock front curves in the downstream direction only near the interface, which is believed to be caused by the large acoustic impedance of granular material compared to that of the gas. This curvature makes the incident angle α_1 of the incident shock waves less than 90°. In addition, under the action of incident shock wave, the transmitted shock wave, induced inside the granular material, makes an oblique angle α_2, and the dusty mass surface behind the shock wave will slope down with a turning angle α_3. These angles, i.e., α_1, α_2 and α_3, are the characteristic parameters used in describing the flowfield induced by shock loading, which can be measured from Fig. 5, and are shown in Fig. 6. In our experiments, the measured values of α_1, α_2 and α_3 are about 89°, 4° and 1–2°, respectively. From Fig. 5b, the oblique interface of the dusty bulk mass is blacker than the adjacent area inside the dust, which indicates that the volume fraction (mass fraction) of particles within that angular area $(\alpha_2 - \alpha_3)$ is higher than that of other areas.

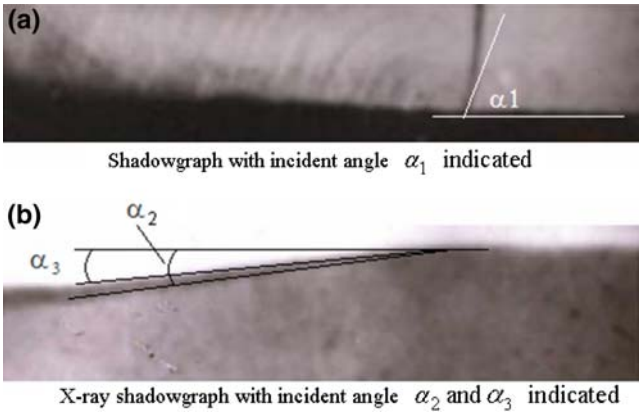

Fig. 6 Measured characteristic parameters of α_1, α_2 and α_3

3 Theoretical investigation

3.1 Mathematical model

The physical phenomenon of the present investigation can be considered as a dense two-phase turbulent flow, thus the mathematical model developed by Gidaspow [10], based on the kinetic theory approach, can be adopted to describe such a flow. In this case, the velocity fluctuation of the dense particle phase is caused by particle–particle collisions rather than the turbulent gas–particle interaction. The fluctuating kinetic energy associated with particle–particle collisions is identified as granular temperature and one equation can be derived for granular temperature based on the the well-known Boltzmann equation

$$\frac{\partial f}{\partial t} + U_{js}\frac{\partial f}{\partial x_j} + F_j\frac{\partial f}{\partial U_{js}} = \left(\frac{\partial f}{\partial t}\right)_{\text{col}}, \tag{1}$$

where f is the frequency distribution of particle velocity and subscript s refers to the particle phase. U_{js} is the instantaneous particle velocity component in the j direction, F_j is the corresponding instantaneous acceleration of particle in the j direction, $(\frac{\partial f}{\partial t})_{\text{col}}$ is related to the particle–particle collisions.

The mean value of a quantity φ is defined to be

$$\langle\varphi\rangle = \frac{\int \varphi f \mathrm{d}\mathbf{U}_s}{\int f \mathrm{d}\mathbf{U}_s}.$$

Hence, the hydrodynamic velocity of particle $\mathbf{u}_s$ becomes

$$\mathbf{u}_s = \frac{\int \mathbf{U}_s f \mathrm{d}\mathbf{U}_s}{\int f \mathrm{d}\mathbf{U}_s}.$$

Then, the granular temperature Θ is defined with

$$\Theta = \frac{1}{3}\left\langle(\mathbf{U}_s - \mathbf{u}_s)^2\right\rangle,$$

which describes the fluctuating velocity of particle phase due to particle–particle collisions. It is common to identity the fluctuation kinetic energy E'_s associated with the granular temperature

$$E'_s = \frac{3}{2}\Theta.$$

The interaction of the fluctuating and mean motion of the particles gives rise to an effective shear viscosity for the particle phase, and the particle material is considered to be incompressible. The governing equations for both gas and particle phases together with the derived constitutive relations are given as follows [10,12].

For the gas phase

$$\frac{\partial(\alpha\rho)_g}{\partial t} + \frac{\partial(\alpha\rho u_i)_g}{\partial x_i} = 0 \tag{2}$$

$$\frac{\partial(\alpha\rho u_j)_g}{\partial t} + \frac{\partial(\alpha\rho u_i u_j)_g}{\partial x_i} = -\alpha_g \frac{\partial p}{\partial x_j} + \frac{\partial \tau_{ij}}{\partial x_i} + V_j \tag{3}$$

$$\begin{aligned}&\frac{\partial(\alpha\rho E)_g}{\partial t} + \frac{\partial(\alpha\rho u_i E)_g}{\partial x_i}\\ &= -(\alpha u_j)_g \frac{\partial p}{\partial x_j} + \frac{\partial[(\alpha u_j)_g + (\alpha u_j)_s]\tau_{ij}}{\partial x_i}\\ &\quad + V_j u_{js} - Q + \frac{\partial}{\partial x_j} k_g \frac{\partial T_g}{\partial x_j}\end{aligned} \tag{4}$$

For the particle phase

$$\frac{\partial \alpha_s}{\partial t} + \frac{\partial(\alpha u_j)_s}{\partial x_j} = 0 \tag{5}$$

$$\begin{aligned}&\frac{\partial(\alpha u_j)_s}{\partial t} + \frac{\partial(\alpha u_i u_j)_s}{\partial x_i}\\ &= -\frac{\alpha_s}{\rho_s}\frac{\partial p}{\partial x_j} + \frac{1}{\rho_s}\frac{\partial \pi_{ij}}{\partial x_i} + \alpha_s g_j - \frac{V_j}{\rho_s}\end{aligned} \tag{6}$$

$$\begin{aligned}&\frac{\partial[\alpha(E+E')]_s}{\partial t} + \frac{\partial[\alpha u_i(E+E')]_s}{\partial x_i}\\ &= -(\alpha u_j)_s \frac{p}{x_j} + \frac{\partial[(\alpha u_j)_g + (\alpha u_j)_s]\pi_{ij}}{\partial x_i}\\ &\quad -\frac{1}{\rho_s} V_j u_{js} + \frac{Q}{\rho_s} + (\alpha u_j)_s g_j\end{aligned} \tag{7}$$

$$\begin{aligned}&\frac{3}{2}\left(\frac{\partial(\alpha\Theta)_s}{\partial t} + \frac{\partial(\alpha\mu_j\Theta)_s}{\partial x_j}\right)\\ &= \frac{\pi_{ij}}{\rho_s}\frac{\partial u_{js}}{\partial x_i} - \frac{1}{\rho_s}\frac{\partial(\Gamma_\theta \frac{\partial\Theta}{\partial x_i})}{\partial x_i} - \frac{\Gamma}{\rho_s},\end{aligned} \tag{8}$$

where subscript g and s denote the gas and particle phase, respectively. α is the volume fraction and $\alpha_s + \alpha_g = 1$, p is the pressure, T is the temperature, u_i is the velocity component in ith direction, g_j is the gravitational acceleration in jth direction, $E = C_v T + u_i u_i/2$ is the internal energy, C_v is the specific heat at constant volume. The gas–phase shear stress is given by

$$\tau_{ij} = \mu_g\left[\left(\frac{\partial u_j}{\partial x_i} + \frac{\partial u_i}{\partial x_j}\right) - \frac{2}{3}\delta_{ij}\frac{u_k}{x_k}\right]_g.$$

According to subgrid-scale (SGS) model [13], the gas phase turbulent shear viscosity can be written as

$$\mu_g = \mu_l + \mu_t = \mu_l + \rho_g(c_t\triangle)^2(\tau_{ij}\cdot\tau_{ij})$$

with

$$c_t = 0.1$$
$$\triangle = \sqrt{\triangle x \triangle y}$$

Based on second approximation of Boltzmann equation and the dense transport theorem, the total stress tensor of particle phase can be expressed as

$$\begin{aligned}\pi_{ij} = &-p_s\delta_{ij} + \mu_s\left[\left(\frac{\partial u_j}{\partial x_i} + \frac{\partial u_i}{\partial x_j}\right) - \frac{2}{3}\delta_{ij}\frac{\partial u_k}{\partial x_k}\right]_s\\ &+ \xi_s\delta_{ij}\left(\frac{\partial u_k}{\partial x_k}\right).\end{aligned}$$

The pressure of particle phase generated by particle–particle collisions can be written as

$$p_s = \alpha_s\rho_s[1 + 2(1+e)\alpha_s g_0]\Theta,$$

which is identical with the state equation of the real gas, where ρ_s is the particle material density, e is the restitution coefficient of inelastic particle and was taken to be 0.995 in present work, the radial distribution function g_0 is given by

$$g_0 = \left[1 - \left(\frac{\alpha_s}{\alpha_{s\,\max}}\right)^{\frac{1}{3}}\right]^{-1}.$$

The shear viscosity of particle phase

$$\mu_s = A_1\mu_{s,\mathrm{dil}} + \alpha_s\mu_{sc},$$

where $\mu_{s,\mathrm{dil}} = \frac{5}{96}\rho_s \mathrm{d}_p\sqrt{\pi\Theta}$ is the dilute phase viscosity [14], d_p is the particle diameter, $\mu_{sc} = \frac{4}{5}\alpha_s\rho_p\mathrm{d}_p g_0(1+e)\sqrt{\frac{\Theta}{\pi}}$ is the Gidaspow viscosity of particle phase.

The modified coefficient for dense phase A_1 and the Gidaspow bulk viscosity of particle phase ξ_s have the following forms

$$A_1 = \frac{2}{(1+e)g_0}(1 + 0.8(1+e)g_0\alpha_s)^2$$

$$\xi_s = \frac{4}{3}\alpha_s^2\rho_s\mathrm{d}_p g_0(1+e)\sqrt{\frac{\Theta}{\pi}}$$

The total conductivity of particle phase can be expressed as

$$\mathbf{\Gamma}_\theta = A_2\mathbf{\Gamma}_{\mathrm{dil}} + \mathbf{\Gamma}_{sc},$$

where the dilute phase granular conductivity [15]

$$\mathbf{\Gamma}_{\mathrm{dil}} = \frac{75}{384}\rho_s \mathrm{d}_p \sqrt{\pi\Theta}.$$

The modified coefficient for dense phase A_2 and the Gidaspow granular conductivity $\mathbf{\Gamma}_{sc}$ have the following forms

$$A_2 = \frac{2}{(1+e)g_0}(1+1.2(1+e)g_0\alpha_s)^2$$

$$\mathbf{\Gamma}_{sc} = 2\alpha_s^2\rho_s \mathrm{d}_p(1+e)g_0\sqrt{\frac{\Theta}{\pi}}$$

The collisional energy dissipation is given by

$$\mathbf{\Gamma} = 3(1-\mathrm{e}^2)\alpha_s^2\rho_s g_0\Theta\left[\frac{4}{\mathrm{d}_p}\sqrt{\frac{\Theta}{\pi}} - \frac{\partial u_{ks}}{\partial x_k}\right].$$

V_j is the momentum transfer between phases in j direction, which is equal to

$$V_j = \beta(u_{gj} - u_{sj}) - f_L,$$

where

$$\beta_j = \begin{cases} 150\frac{\alpha_s^2\mu_g}{\alpha_g \mathrm{d}_p^2} + 1.75\frac{\alpha_s\rho_g|u_{gj}-u_{sj}|}{\mathrm{d}_p} & \alpha_g < 0.8 \\ \frac{3}{4}C_D\frac{\alpha_s\rho_g|u_{gj}-u_{sj}|}{\mathrm{d}_p}\alpha_g^{-1.65} & \alpha_g \geq 0.8 \end{cases}$$

$$C_D = \begin{cases} \frac{24}{R_e}(1+0.15{R_e}^{0.678}) & R_e \leq 1{,}000 \\ 0.44 & R_e > 1{,}000 \end{cases}$$

$$R_e = \frac{\alpha_g\rho_g \mathrm{d}_p|\overrightarrow{u_g} - \overrightarrow{u_s}|}{\mu_l}$$

$F_L = \mathrm{Sgn}(\frac{\partial u_g}{\partial y})\frac{3K\alpha_s}{2\pi \mathrm{d}_p}(u_g - u_s)\sqrt{(\rho\mu)_g|\frac{\partial u_g}{\partial y}|}$ is the lift force.

Q is the energy transfer between phases,

$$Q = \frac{6}{\mathrm{d}_p^2}N_u k_g \alpha_s(T_g - T_s),$$

where Nusselt number $N_u = 2 + 0.6P_r^{\frac{1}{3}}\mathbf{R_e}^{\frac{1}{2}}$, k_g is gas thermal conductivity, P_r is Prandtl number.

3.2 Numerical method

The AUSM scheme [11] has the advantage of capturing shock waves efficiently, avoiding complicated matrix operations and extending easily to treat other hyperbolic systems. In addition, it is very simple to construct and more efficient than other methods in dealing with a large set of equations in hyperbolic systems such as those described above, therefore, it was employed in present calculations. A one-dimensional system of Euler equations for a perfect gas is used to exemplify this scheme as follows:

$$\frac{\partial \mathbf{U}}{\partial t} + \frac{\partial \mathbf{F}}{\partial x} = 0, \tag{9}$$

where $\mathbf{U} = (\rho, \rho u, \rho E)^{\mathrm{T}}$ and the flux vector $\mathbf{F} = (\rho u, \rho u^2 + p, \rho u H)^{\mathrm{T}}$, in which E is the specific total energy and H is the specific total enthalpy.

The flux vector $\mathbf{F}$ consists of two physically distinct parts, namely convective and pressure fluxes,

$$\mathbf{F} = \mathbf{F^c} + \mathbf{P}, \tag{10}$$

where the convective flux $\mathbf{F^c} = Ma\mathbf{\Phi}$, M is Mach number, a is the sound speed, $\mathbf{\Phi} = (\rho, \rho u, \rho H)^{\mathrm{T}}$ is a vector with scalar quantities, the pressure flux $\mathbf{P} = (0, p, 0)^{\mathrm{T}}$. For the numerical solution, we discretize two components separately. Hence, the flux vector at an interface between the numerical cells j and $j+1$ can be written as

$$\mathbf{F}_{j+\frac{1}{2}} = M_{j+\frac{1}{2}}(a\mathbf{\Phi})_{L/R} + \mathbf{P}_{j+\frac{1}{2}}, \tag{11}$$

where

$$\mathbf{P}_{j+\frac{1}{2}} = (0, p_{j+\frac{1}{2}}, 0)\ (\bullet)_{L/R} = \begin{cases} (\bullet)_L & \text{if } M_{j+\frac{1}{2}} \geq 0 \\ (\bullet)_R & \text{otherwise} \end{cases}$$

$M_{j+\frac{1}{2}}$ and $\mathbf{P}_{j+\frac{1}{2}}$ are written as two individual components,

$$M_{j+\frac{1}{2}} = M_j^+ + M_{j+1}^- \tag{12}$$

$$P_{j+\frac{1}{2}} = fP_j^+ p_j + P_{j+1}^- p_{j+i} \tag{13}$$

where

$$M^{\pm} = \begin{cases} \frac{1}{2}(M + |M|) & |M| \geq 1 \\ \pm\frac{1}{4}(M \pm 1)^2 \pm \frac{1}{8}(M^2-1)^2 & |M| < 1 \end{cases}$$

$$P^{\pm} = \begin{cases} \frac{1}{2}(1 \pm \mathrm{sign}(M)) & |M| \geq 1 \\ \frac{1}{4}(M \pm 1)^2(2 \mp M) \pm \frac{3}{6}M(M^2-1)^2 & |M| < 1 \end{cases}$$

In present investigation, the conservation equations of dense two-phase turbulent flow described above are solved numerically by using the AUSM scheme in which it is necessary to derive the formulations of sound speed in the gas and particle phases seperately. For the gas phase, the Jacobian matrix of conservation equations is given by

$$\mathbf{A} = \frac{\partial \mathbf{F}}{\partial \mathbf{U}} = \begin{pmatrix} 0 & 1 & 0 & 0 \\ a_{21} & a_{22} & 0 & 0 \\ a_{31} & a_{32} & a_{33} & 0 \\ a_{41} & a_{42} & 0 & a_{44} \end{pmatrix}$$

where $a_{22} = 2u_g$, $a_{33} = a_{44} = u_g$, $a_{21} = (1 - \frac{\alpha_s}{\gamma})a_0^2 - u_g^2$, a_0 is the sound speed in pure gas, γ is the adiabatic index,

the eigenvalue vector of Jacobian matrix **A** is written as

$$\boldsymbol{\lambda} = \begin{pmatrix} u_g \\ u_g \\ u_g + a_g \\ u_g - a_g \end{pmatrix}$$

where $a_g = \sqrt{u_g^2 + a_{21}} = a_0\sqrt{1 - \frac{\alpha_s}{\gamma}}$ is the sound speed in gas phase.

In the same way, the sound speed in particle phase α_s can be derived as follows:

$$\alpha_s = \sqrt{\frac{p}{\rho_s} + \frac{\alpha_g \Theta(1+e)g_0}{3}\left(6 + \frac{10}{3}g_0\left(\frac{\alpha_s}{\alpha_{(s\,\max)}}\right)^{\frac{1}{3}}\right) + \Theta(1+2(1+e)\alpha_s)g_0}$$

4 Results and discussion

It is assumed in our calculations that the shock wave with Mach number $M_s = 2$ impinges on the dusty bulk at an initial time $t = 0$. The initial conditions are the same with those in experiments. The calculated results at time $t = 7.45$ are shown in Figs. 7 and 8.

The density contour of gas in the air and the dusty mass under the interaction of the shock wave are shown in Fig. 7a, from which the curve of the incident shock wave near impinging points and the turning of the transmitted shock waves can be seen clearly. Figure 7b displays the temperature distribution of gas. It is clear that a considerable change of temperature occurs in the air behind the incident shock wave. From the total pressure distribution in Fig. 7c, the oblique angle of the incident shock wave α_1, the transmitted shock oblique angle α_2 and the turning angle α_3 can be observed clearly. Combined with the experimental results of Figs. 5b and 6b, it can be concluded that the reason for the formation of an oblique dust interface with a high volume fraction behind the shock wave is due to the existence of high pressure in this area.

The granular temperature, thermal temperature and volume fraction distributions of particles are shown in Fig. 8. The fluctuating motion of the particles occurs mainly in the region behind the transmitted shock wave near the dusty bulk mass, which also dominates the collision pressure, the collisional momentum transfer and the granular conductivity (Fig. 8a). From the distribution of particle thermal temperature (Fig. 8.b), only the temperature of particles suspended in air increases significantly and the temperature inside the dusty bulk is almost constant. The volume fractions of particles vary significantly due to the action of the shock wave (Fig. 8c), and attains its highest value on the oblique interface

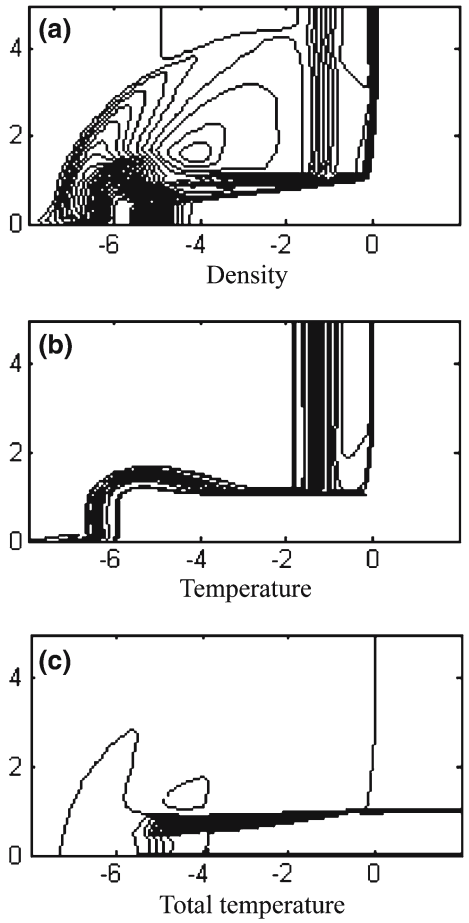

Fig. 7 Contours of flowfield in gas phase at $t = 7.45$

behind the shock wave. This agrees well with our experimental results (Figs. 5b, 6b). Both in Figs.7 and 8, the shape of the dusty mass surface and the transmitted shock wave was shown and is comparable with our measured results.

The velocity vector plot of gas and particles is shown in Fig.9. Under the influence of shock waves, particles in the region between the original dust surface and the transmitted wave will move down due to the compression of dusty mass, and particles above the dust surface will go up under the action of the lifting force.

The variation of characteristic angles in the flowfield, i.e., α_1, α_2 and α_3, along with the propagating velocity (intensity) of the incident shock wave q_0 are shown in Fig.10a–c, respectively. The discrete point '$*$' represents the experimental value while the solid line shows our calculated results. The oblique angle of the incident shock wave α_1 increases with the rise of the incident shock propagation velocity. However, the compressed region in the dusty bulk mass behind the incident shock is reduced with increasing propagation velocity of the incident shock wave because of the increase of the

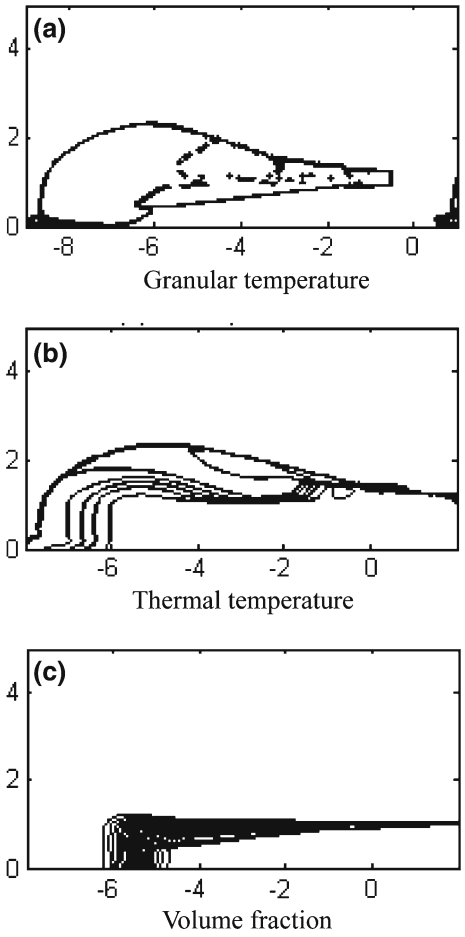

Fig. 8 Contours of flowfield in particle phase at $t = 7.45$

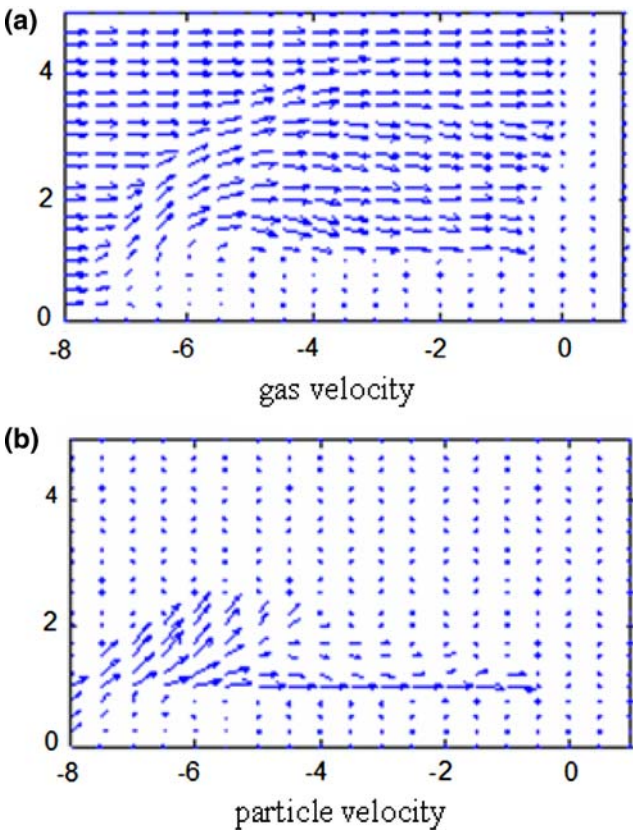

Fig. 9 Velocity vectors

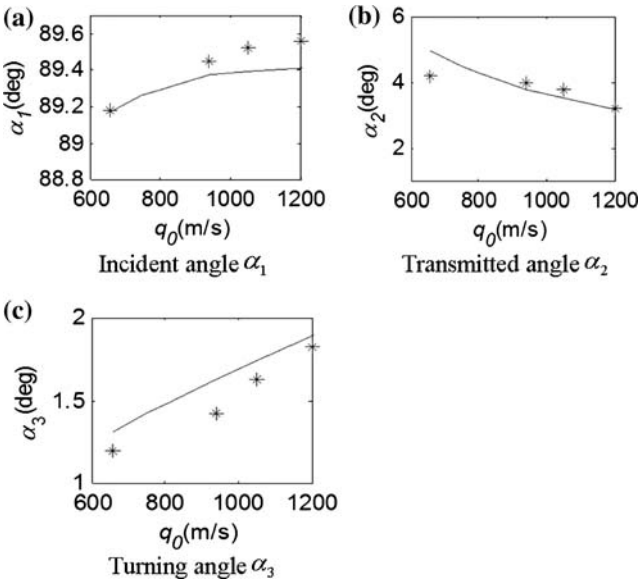

Fig. 10 Variations of incident angle α_1, transmitted shock oblique angle α_2 and turning angle α_3 with shock velocity q_0. *Solid line* calculated, *asterisks* measured

turning angle α_2 and the decrease of the transmitted shock angle α_3.

5 Conclusions

In the present investigation, the complex phenomenon of a shock wave interacting with a dusty bulk mass has been studied both experimentally and numerically.

A specific experimental setup, including measurement technology, has been developed for visualization of this phenomenon. The flowfield of the gas and granular phases has been visualized by means of shadowgraphs and pulsed X-ray shadowgraphs with trace particles. Three characteristic angles, the incident angle of the incident shock, the oblique angle of the transmitted shock wave and the turning angle of the dusty mass surface behind the shock wave have been measured.

The dense two-phase flow model developed by Gidaspow [10] from the kinetic theory, has proven to be valid for the description of the interaction of a shock wave with a dusty mass layer. The AUSM scheme adopted in the present work has also been proven suitable for the solution of the partial differential equations of a dense two-phase flow. The numerical results

are in good agreement with corresponding measured results. They show that the fluctuating motion of the particles, which dominates the collision pressure, the collisional momentum transfer and the granular conductivity, occurs mainly in the region behind the transmitted shock wave near the dusty bulk mass. The temperature of the particles suspended in air increases significantly, while the temperature inside the dusty bulk remains almost constant. The particle volume fraction varies significantly due to the action of the shock wave. It attains its highest value on the oblique interface behind the shock wave.

Acknowledgements The authors of this paper are grateful for the support provided by the National Science Foundation of China under Grant No. 19772018 and 50376024

References

1. Fletcher, B.: The interaction of a shock with a dust deposit. J. Phys. D Appl. Phys. **9**,197–202 (1976)
2. Gelfand, BE., Medvedev, SP., Borisov, AA., Polenov, AN., Frolov, SM., Tsyganov, SA.: Shock loading of stratified dusty systems. Arch. Combust. **9**(4), 153–165 (1989)
3. Fan, B., Li, H.: Detonation supported by combustible dust deposit. In: Proceedings of the 26th International Symposium on Combustion, Napoles, Italia, pp. 3007-3013. The Combustion Institute, Pittsburgh (1996)
4. Li, H., Fan, B., Geng, J., Lu, S.: Shock wave interaction with surface of combustible dust layers. Sci. China E **39**(5), 449-460 (1996)
5. Thevand, N., Daniel, E.: Numerical study of the lift force influence on two-phase shock tube boundary layer characteristics. Shock Waves **11**, 279–288 (2002)
6. Katsunori, D., Igor, M., Yoshiaki, N.: Numerical simulation of interaction between moving shock wave and solid particle layer. AIAA, 2002–3180 (2002)
7. Baer, MR., Nunziato, JW.: A two-phase mixture theory for the deflagration-to-detonation transition (DDT) in reactive granular materials. Int J Multiphase Flow **12**, 861–889 (1986)
8. Powers, JM., Stewart, DS., Krier, H.: Theory of two-phase detonations part I: modeling. Combust. Flame **80**, 264–279 (1990)
9. Zhang, F., Frost, DL., Thibault, PA., Murray, SB.: Explosion dispersal of solid particles. Shock Waves **10**, 431–443 (2001)
10. Gidaspow, D.: Multiphase flow and fluidization. Academic Press, San Diego (1994)
11. Liou, MS.: Progress towards and improved method: AUSM+. AIAA, 95–1701 (1995)
12. Soo, SL.: Multiphase fluid dynamics. Science Press, Beijing (1990)
13. Deardorff, JW.: On the magnitude of the sub grid scale eddy coefficient. J. Comput. Phys. **7**, 120–135 (1971)
14. Chapman, S., Cowling, TG.: The mathematical theory of non-uniform gases. Cambridge University Press, Cambridge (1961)
15. Lun, CKK., Savage, SB., Jeffrey, DJ., Chepumiy, N.: Kinetic theories for granular flow: inelastic particles in couette flow and singly inelastic particles in a general flow field. J. Fluid Mech. **140**, 223–256 (1984)